Scientia Iranica (2024) 31(8), 632–645

Sharif University of Technology
Scientia Iranica
Transactions B: Mechanical Engineering
https://scientiairanica.sharif.edu

Peristaltic motion of non-Newtonian fluid under the influence of inclined magnetic field, porous medium, and chemical reaction

R. Vijayaragavan[a], P. Tamizharasi[a,1], and A. Magesh[b,2,*]

a. *Thiruvalluvar University, Serkadu,, Vellore, Tamilnadu, 632 115, India.*
b. *JEI Mathaajee College of Engineering, Kanchipuram, 631 552, India.*
1. *Present address: Easwari Engineering College, Ramapuram, Chennai 600 089, India.*
2. *Present address: Sri Sai Ram Engineering College, Chennai 600 044, India.*

Received 30 November 2021; received in revised form 28 January 2023; accepted 24 January 2024

KEYWORDS
Inclined magnetic field;
Peristaltic transport;
Porous medium;
Slip parameters.

Abstract. In this article, we studied the peristaltic motion of Jeffrey fluid with the porous medium through an asymmetric channel under the influence of velocity slip parameters. Governing equations for non-Newtonian fluid flow models, such as continuity, momentum, energy, and mass transfer, are formulated. An externally applied inclined magnetic field is also considered in the flow pattern. The lengthy governing equation of fluid motion is reduced by considering the approximation of longer wavelengths and smaller Reynolds numbers. ($Re \to 0$). The resulting governing equations are solved exactly. The graph shows the results of the impact of various related fluid parameters such as Hartmann number, Darcy number, Jeffrey fluid parameter, amplitude ratio, chemical reactions of fluid velocity, temperature, concentration, pressure rise, pressure gradient, streamlines, etc. Finally, the various waveforms of the trapping phenomenon are presented.

1. Introduction

The peristaltic movement of non-Newtonian and Newtonian fluids has received particular attention for its wide applications in physiology, engineering, and modern industry. In physiological terms, urine transport to the bladder through the kidney, in the ingestion of food via the esophagus, capillaries and arterioles, vasomotion of venues, in the unsanitary transport of fluids, in the movement of worms, transport of toxic fluids in the nuclear industry, roller, finger pumps. Latham made the initial attempt at peristaltic transport [1]. Brown and Hung [2] investigated nonlinear two-dimensional peristaltic transportation using experimental and computational methods. The peristaltic movement through an inclined tube of Herschel-Bulkley fluid has been described by Vajravelu et al. [3].

*. *Corresponding author.*
E-mail address: mageshmaths86@gmail.com (A. Magesh)

To cite this article:
R. Vijayaragavan, P. Tamizharasi, and A. Magesh "Peristaltic motion of non-Newtonian fluid under the influence of inclined magnetic field, porous medium, and chemical reaction", *Scientia Iranica* (2024), **31**(8), pp. 632-645
DOI: 10.24200/sci.2024.59484.6270

Wang et al. [4] discussed the Johnson Segalman fluid through peristalsis in the deformable tube. A few studies on the peristaltic mechanism of different fluid patterns are presented [5–8].

The study of the peristaltic transport of MHD (magnetohydrodynamic) has special attention due to its numerous applications in electricity production, bioengineering, and medicine. In particular, it finds utility in blood pumps, generator sets, MHD compressor operation, flow meters, radar systems, heat exchanger construction, etc. MHD dust fluid through Peristaltic transport was described by Muthuraj et al. [9]. They employed an analytic solution to solve the equations of solids and liquids and reported that the appearance of magnetic parameters on the transverse side creates the drag force and affects the movement of the liquid in the opposite direction, causing the velocity to decrease. A few studies of peristaltic motion with MHD in different fluids under different boundary conditions are presented [10–14].

Porous materials provide significant advantages in comparison with conventional construction. The non-uniform flow of fluids ensures that fluids are uniformly blended and also supports them in maintaining the temperature distribution. Mathematically, the flow rate in the porous medium is defined by Darcy's law [15]. He indicated that the flow rate is directly proportional to the pressure gradient and the flow cross-section. Some studies based on the presence of porous media across different fluid flow patterns in different flow geometries can be found in [16–25]. Nadeem et al. [26] discussed the peristaltic movement of Jeffrey nanofluid in rectangular ducts. Blood clots are a major cause of various illnesses around the world, like heart attacks; stroke is the main element behind death, as addressed by Bhatti et al. [27]. Bhatti et al. [28] discussed the mobility of intrauterine particles along an asymmetric tapered conduit with heat transfer. Magesh and Kothandapani [29] examined the power and mass transfer analysis of the Johnson Segalmann fluid in an asymmetric channel.

All studies above, but few in the available literature, on the impact of velocity second slip conditions on the peristaltic movement in a channel/tube. According to available literature, no effort has been made to investigate the influence of velocity second slip conditions through the peristaltic mechanism of Jeffrey fluid in an inclined asymmetric channel. Thus, the present study proposes to construct the work on the impact of velocity second slip parameters of the peristaltic movement of Jeffrey fluid. Additionally, its consider has the impact of inclined magnetic field, porous medium and chemical reaction. Mass and energy transfer of the fluid was also studied. The exact solutions are derived from the simplified governing equations. The influence of various fluid parameters on the flow characteristics is analyzed by means of graphic illustrations.

2. Formulation of the present problem

We consider viscous, incompressible, unsteady two-dimensional Jeffrey fluid induced by a peristaltic system through an asymmetrical channel enclosed by $\bar{h}_1(\widehat{X}', \widehat{t}')$ and $\bar{h}_2(\widehat{X}', \widehat{t}')$. The fluid is considered to drive electrically in the appearance of an inclined magnetic field and porous medium. The flow generates sinusoidal waves propagating at a non-varying speed through the channel walls. Asymmetry of the channel due to phase difference (see Figure 1) is represented by [30,31]:

$$\bar{h}_1 = -d_2 - b_1 \cos\left[\frac{2\pi\left(\widehat{X}' - c\widehat{t}'\right)}{\lambda} + \phi\right],$$

$$\bar{h}_2 = d_1 + a_1 \cos\left[\frac{2\pi\left(\widehat{X}' - c\widehat{t}'\right)}{\lambda}\right], \tag{1}$$

where $d_1 + d_2$, ϕ, a_1, b_1 are the channel width, phase difference, and amplitudes of the waves. ϕ changes in the range $0 \le \phi \le \pi$ the channel is symmetric at $\phi = 0$ (waves out of phase), and the waves are in phase at $\phi = \pi$, λ is the wavelength, and further b_1, a_1, d_2, d_1, and ϕ satisfies as the following relation is:

$$b_1^2 + a_1^2 + 2b_1 a_1 \cos\phi \le (d_2 + d_1)^2. \tag{2}$$

The extra stress tensor $\bar{S}$ and stress tensor $\bar{\tau}$ of the Jeffrey model are [25]:

$$\bar{\tau} = -PI + \bar{S}, \tag{3}$$

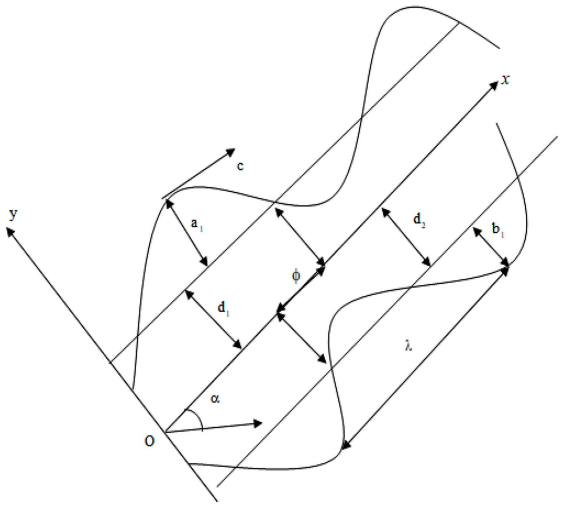

Figure 1. Physical model of the channel.

$$\bar{S} = \frac{\mu}{1+\lambda_1}\left(\dot{\gamma} + \lambda_2 \ddot{\gamma}\right),$$

where λ_1, λ_2, μ, $\dot{\gamma}$, and $\ddot{\gamma}$ are the constants of Jeffrey fluid, coefficient of fluid viscosity, and shear stress, and the dot over the quantities denotes the derivative with respect to time t. P is the pressure, and I is the identity tensor.

2.1. Assumptions

Reynolds number: The gastrointestinal or reproductive tracts essentially have a creeping flow of fluid. The Reynolds number is, therefore, extremely low (1 for the ureter, 10 for the gastrointestinal tract). Comparing the momentum equation to the linear viscous forces, the inertia term, which is proportional to the square of velocity, can be neglected.

Wavelength: It should be noted that the vas deferens radius is extremely small in comparison to the wavelength. Because the wave number is typically low, this situation can benefit from the long wavelength approximation theory [8].

2.2. Governing equations

The governing equations of non-Newtonian fluids, such as continuity, momentum, energy, and concentration equations, are as follows [10,30]:

$$\frac{\partial \widehat{U}'}{\partial \widehat{X}'} + \frac{\partial \widehat{V}'}{\partial \widehat{Y}'} = 0. \tag{4}$$

$$\rho\left(\frac{\partial \widehat{U}'}{\partial \widehat{t}'} + \frac{\partial \widehat{U}'}{\partial \widehat{X}'}\widehat{U}' + \widehat{V}'\frac{\partial \widehat{U}'}{\partial \widehat{Y}'}\right) = -\frac{\partial P}{\partial \widehat{X}'} + \frac{\partial \bar{S}_{\bar{x}\bar{x}}}{\partial \widehat{X}'} + \frac{\partial \bar{S}_{\bar{x}\bar{y}}}{\partial \widehat{Y}'} - \sigma_0 B_0^2 \cos\Omega\left(\cos\Omega\,\widehat{U}' - \sin\Omega\,\widehat{V}'\right) - \frac{\mu}{k_1}\widehat{U}' + g\rho\sin\alpha, \tag{5}$$

$$\rho\left(\frac{\partial \widehat{V}'}{\partial \widehat{t}'} + \frac{\partial \widehat{V}'}{\partial \widehat{X}'}\widehat{U}' + \frac{\partial \widehat{V}'}{\partial \widehat{Y}'}\widehat{V}'\right) = -\frac{\partial P}{\partial \widehat{Y}'} + \frac{\partial \bar{S}_{\bar{x}y}}{\partial \widehat{X}'} + \frac{\partial \bar{S}_{\bar{y}\bar{y}}}{\partial \widehat{Y}'} - \frac{\mu}{k_1}\widehat{V}' + \sigma_0 B_0^2 \sin\Omega\left(\cos\Omega\,\widehat{U}' - \sin\Omega\,\widehat{V}'\right) - g\rho\cos\alpha, \tag{6}$$

$$\rho c_p\left(\frac{\partial T}{\partial \widehat{t}'} + \frac{\partial T}{\partial \widehat{X}'}\widehat{U}' + \frac{\partial T}{\partial \widehat{Y}'}\widehat{V}'\right) = \kappa_t\left(\frac{\partial^2 T}{\partial \widehat{X}'^2} + \frac{\partial^2 T}{\partial \widehat{Y}'^2}\right) + \mu\left(\frac{1}{1+\lambda_1}\left(1+\lambda_2\left(\frac{\partial}{\partial \widehat{t}'} + \widehat{U}'\frac{\partial}{\partial \widehat{X}'} + \widehat{V}'\frac{\partial}{\partial \widehat{Y}'}\right)\right)\left(2\left(\frac{\partial \widehat{U}'}{\partial \widehat{X}'}\right)^2 + 2\left(\frac{\partial \widehat{V}'}{\partial \widehat{Y}'}\right)^2 + \left(\frac{\partial \widehat{U}'}{\partial \widehat{Y}'} + \frac{\partial \widehat{V}'}{\partial \widehat{X}'}\right)^2\right)\right), \tag{7}$$

$$\frac{\partial C}{\partial \widehat{t}'} + \widehat{U}'\frac{\partial C}{\partial \widehat{X}'} + \widehat{V}'\frac{\partial C}{\partial \widehat{Y}'} = D_m\left(\frac{\partial^2 C}{\partial \widehat{X}'^2} + \frac{\partial^2 C}{\partial \widehat{Y}'^2}\right) + \frac{D_m K_T}{T_m}\left(\frac{\partial^2 T}{\partial \widehat{X}'^2} + \frac{\partial^2 T}{\partial \widehat{Y}'^2}\right) - k_0(C - C_0), \tag{8}$$

where $\widehat{V}'$ and $\widehat{U}'$ are the velocities on the directions of transverse and axial side, p, $\widehat{t}'$, $\rho, \mu, \sigma_0, c_p, k_1, S_{ij}, \Omega, \kappa_t$, and k_0 represent the pressure, time, density, viscosity, electrical conductivity, specific heat at constant pressure, permeability parameter, extra stress tensor, inclination angle, thermal conductivity, chemical reaction parameter, and B_0 is the applied magnetic field.

The extra stress tensor (S_{ij}) of the Jeffrey fluid model is as follows [14,27,30]:

$$S_{xx} = \frac{2\mu}{1+\lambda_1}\left[1+\lambda_2\left(\frac{\partial}{\partial \widehat{t}'} + \widehat{U}'\frac{\partial}{\partial \widehat{X}'} + \widehat{V}'\frac{\partial}{\partial \widehat{Y}'}\right)\right]\frac{\partial \widehat{U}'}{\partial \widehat{X}'}, \tag{9}$$

$$S_{xy} = \frac{\mu}{1+\lambda_1}\left[1+\lambda_2\left(\frac{\partial}{\partial \widehat{t}'} + \widehat{U}'\frac{\partial}{\partial \widehat{X}'} + \widehat{V}'\frac{\partial}{\partial \widehat{Y}'}\right)\right]\left(\frac{\partial \widehat{U}'}{\partial \widehat{Y}'} + \frac{\partial \widehat{V}'}{\partial \widehat{X}'}\right), \tag{10}$$

$$S_{yy} = \frac{2\mu}{1+\lambda_1}\left[1+\lambda_2\left(\frac{\partial}{\partial \widehat{t}'} + \widehat{U}'\frac{\partial}{\partial \widehat{X}'} + \widehat{V}'\frac{\partial}{\partial \widehat{Y}'}\right)\right]\frac{\partial \widehat{V}'}{\partial \widehat{Y}'}. \tag{11}$$

The flow of the fluid is unsteady in the wave frame. So, it's converted into steady flow by the following transform (wave frame to fixed frame) [7,12]:

$$v' = \widehat{V}' \qquad u' = \widehat{U}' - c,$$

$$y' = \widehat{Y}', \qquad x' = \widehat{X}' - c\widehat{t}'. \tag{12}$$

Introducing the dimensionless variables is as follows:

$$x=\frac{x'}{\lambda},\qquad u=\frac{u'}{c},\qquad y=\frac{y'}{d_1},\qquad h_1=\frac{\bar{h}_1}{d_1},$$

$$h_2=\frac{\bar{h}_2}{d_1},\qquad t=\frac{c\bar{t}}{\lambda},\qquad b=\frac{b_1}{d_1},\qquad a=\frac{a_1}{d_1},$$

$$d=\frac{d_2}{d_1},\qquad v=\frac{v'}{c\delta},\qquad {S_{ij}}^*=\frac{d_1 S_{ij}}{c\mu},$$

$$\theta=\frac{T-T_0}{T_1-T_0},\qquad p=\frac{d_1^2}{\mu\lambda c}\bar{P},\qquad \sigma=\frac{C-C_0}{C_1-C_0}. \tag{13}$$

In which $Re=\frac{\rho c d_1}{\mu}$ is Reynolds number, a and b are amplitudes of the waves, $\delta=\frac{d_1}{\lambda}$ is wave number, $E=\frac{c^2}{c_p(T_1-T_0)}$ is Eckert number, $M=\sqrt{\frac{\sigma_0}{\mu}}B_0 d_1$ is Hartmann number, $Pr=\frac{\mu c_p}{\kappa_t}$ is the Prandtl number, $Da=\frac{k_1}{d_1^2}$ is Darcy number, $Sr=\frac{\rho D_m(T_1-T_0)K_T}{\mu T_m(C_1-C_0)}$ is Soret number, $Br=EPr$ is Brinkmann number, $Sc=\frac{\mu}{\rho D_m}$ is Schmidt number, $\gamma_1=\frac{\rho k_0 d_1^2}{\mu}$ is the chemical reaction parameter, and $Fr=\frac{c^2}{g d_1}$ is Froude number.

Applying Eqs. (12) and (13) into Eqs. (4)–(11), Eq. (4) is fully satisfied. Under the assumptions of lubrication theory, Eqs. (5)–(8) becomes:

$$\frac{\partial p}{\partial x}=\frac{\partial S_{xy}}{\partial y}-M^2\cos^2\Omega(u+1)$$
$$-\frac{1}{Da}(u+1)+\frac{Re}{Fr}\sin\alpha, \tag{14}$$

$$\frac{\partial p}{\partial y}=0, \tag{15}$$

$$\frac{1}{Pr}\frac{\partial^2\theta}{\partial y^2}+\frac{E}{1+\lambda_1}\left(\frac{\partial u}{\partial y}\right)^2=0, \tag{16}$$

$$\frac{1}{Sc}\frac{\partial^2\sigma}{\partial y^2}+Sr\frac{\partial^2\theta}{\partial y^2}-\gamma_1\sigma=0. \tag{17}$$

The stream functions are:

$$v=-\delta\frac{\partial\psi}{\partial x},\ u=\frac{\partial\psi}{\partial y}. \tag{18}$$

Eqs. (14) and (16) in terms of stream function ψ can be rewritten by:

$$\frac{\partial p}{\partial x}=\frac{1}{1+\lambda_1}\frac{\partial^3\psi}{\partial y^3}-\left(M^2\cos^2\Omega+\frac{1}{Da}\right)\left(\frac{\partial\psi}{\partial y}+1\right)$$
$$+\frac{Re}{Fr}\sin\alpha, \tag{19}$$

$$\frac{\partial^2\theta}{\partial y^2}+\frac{Br}{1+\lambda_1}\left(\frac{\partial^2\psi}{\partial y^2}\right)^2=0, \tag{20}$$

$$\frac{\partial^2\sigma}{\partial y^2}+ScSr\frac{\partial^2\theta}{\partial y^2}-Sc\gamma_1\sigma=0. \tag{21}$$

From Eq. (15), we conclude that pressure is independent of y. Now, eliminating the pressure gradient in Eq. (19) and differentiating partially with respect to y, we get:

$$\frac{\partial^4\psi}{\partial y^4}-A_1^2\frac{\partial^2\psi}{\partial y^2}=0. \tag{22}$$

The corresponding boundary conditions of slip conditions are [30]:

$$\psi=-\frac{F}{2}\quad\text{and}$$

$$\frac{\partial\psi}{\partial y}=\frac{\bar{\eta}_1}{(1+\lambda_1)}\frac{\partial^2\psi}{\partial y^2}+\frac{\bar{\eta}_2}{(1+\lambda_1)}\frac{\partial^3\psi}{\partial y^3}-1\quad\text{at}$$

$$y=h_1[=-b\cos(2\pi x+\phi)-d],\psi=\frac{F}{2}\quad\text{and}$$

$$\frac{\partial\psi}{\partial y}=-\frac{\bar{\eta}_1}{(1+\lambda_1)}\frac{\partial^2\psi}{\partial y^2}-\frac{\bar{\eta}_2}{(1+\lambda_1)}\frac{\partial^3\psi}{\partial y^3}-1\quad\text{at}$$

$$y=h_2[=a\cos(2\pi x)+1], \tag{23}$$

$$\theta+\beta\frac{\partial\theta}{\partial y}=0\quad\text{at}\quad y=h_1\quad\text{and}$$

$$\theta-\beta\frac{\partial\theta}{\partial y}=1\quad\text{at}\quad y=h_2, \tag{24}$$

$$\sigma+\gamma\frac{\partial\sigma}{\partial y}=0\quad\text{at}\quad y=h_1$$

$$\text{and}\quad\sigma-\gamma\frac{\partial\sigma}{\partial y}=1\quad\text{at}\quad y=h_2, \tag{25}$$

where F is the flux, $\bar{\eta}_1,\bar{\eta}_2,\beta$, and γ represent first order, second order, thermal, and concentration slip parameters, respectively, and b,a,d, and ϕ satisfies the condition:

$$b^2+a^2+2ba\cos\phi\le(1+d)^2.$$

3. Solution of the present flow pattern

The exact solution of Eqs. (20)–(22) is obtained with the help of Eqs. (23)–(25):

$$\psi=c_1+c_2y+c_3\cosh A_1y+c_4\sin A_1y, \tag{26}$$

$$\theta=c_5+c_6y+\frac{A_{14}e^{2A_1y}}{4A_1^2}+\frac{A_{15}e^{-2A_1y}}{4A_1^2}+A_{16}\frac{y^2}{2}, \tag{27}$$

$$\sigma=c_7\cosh(\sqrt{Sc\gamma_1}y)+c_8\sinh(\sqrt{Sc\gamma_1}y)$$
$$-ScSr\left(\frac{A_{14}e^{2A_1y}+A_{15}e^{-2A_1y}}{4A_1^2-Sc\gamma_1}-\frac{A_{16}}{Sc\gamma_1}\right), \tag{28}$$

where c_i, $i = 1-8$, are constants presented in the appendix.

Substitution Eq. (26) into Eq. (19) gives the pressure gradient in the axial direction:

$$\frac{\partial p}{\partial x} = \frac{1}{1+\lambda_1} A_1^3 c_4 - A_1^2 \left(c_2 + A_1 c_4 + 1\right) + \frac{Re}{Fr} \sin\alpha. \tag{29}$$

The pressure rise is calculated numerically per wavelength by the following formula:

$$\Delta p_\lambda = \int_0^{2\pi} \frac{dp}{dx} dx. \tag{30}$$

The possible wave shapes namely, Sawtooth, Trapezoidal, Triangular, and Square waveforms, are modeled from the Fourier series as follows [8]:

- Sawtooth waveform:

$$h_1 = 1 + a\frac{8}{\pi^3} \sum_{j=1}^{\infty} \frac{\sin(2j\pi x)}{j},$$

$$h_2 = -d - b\frac{8}{\pi^3} \sum_{j=1}^{\infty} \frac{\sin\left[(2j\pi x) + \phi\right]}{j}.$$

- Trapezoidal waveform:

$$h_1 = 1 + a\frac{32}{\pi^2} \sum_{j=1}^{\infty} \frac{\sin\frac{\pi}{8}(2j-1)}{(2j-1)^2} \sin[2\pi(2j-1)x],$$

$$h_2 = -d - b\frac{32}{\pi^2} \sum_{j=1}^{\infty} \frac{\sin\frac{\pi}{8}(2j-1)}{(2j-1)^2} \sin[2\pi(2j-1)x + \phi].$$

- Triangular waveform:

$$h_1 = 1 + a\frac{8}{\pi^3} \sum_{j=1}^{\infty} \frac{(-1)^{j+1} \sin[2\pi(2j-1)x]}{(2j-1)^2},$$

$$h_2 = -d - b\frac{8}{\pi^3} \sum_{j=1}^{\infty} \frac{(-1)^{j+1} \sin[2\pi(2j-1)x + \phi]}{(2j-1)^2}.$$

- Square waveform:

$$h_1 = 1 + a\frac{4}{\pi} \sum_{j=1}^{\infty} \frac{(-1)^{j+1} \cos[2\pi(2j-1)x]}{(2l-1)},$$

$$h_2 = -d - b\frac{4}{\pi} \sum_{j=1}^{\infty} \frac{(-1)^{j+1} \cos[2\pi(2j-1)x + \phi]}{(2j-1)}.$$

4. Result and discussion

The graphical result of velocity, pressure rise, pressure gradient, temperature, and concentration profiles are plotted using the computational mathematical software Matlab, and the streamlines are drawn using Mathematica.

4.1. Velocity profile

Figure 2(a)–(d) presents variations of the velocity profile (u) for changing the values of M (Hartmann number), Da (Darcy number), λ_1 (Jeffrey fluid parameter), and ϕ (phase difference). Figure 2(a) indicates that when the Hartmann number increases, the velocity of the fluid decreases in the middle of the porous channel. However, reverse behavior occurred near the channel's walls. That means a larger magnetic field declines the fluid velocity in the axial direction as Lorentz force plays retarding force in the fluid movement [32,33]. Figure 2(b) illustrates the impact of Darcy number Da on the velocity profile. This figure suggests that increasing Da means diminishing the drag force, and that causes enhance the axial velocity. Figure 2(c) shows the impact of Jeffrey fluid parameter λ_1. From this figure, we concluded that the axial velocity diminishes for greater λ_1. Also, it is observed that in the case of Newtonian fluid ($\lambda_1 = 0$), the velocity is maximum. The fluid velocity reduces near the left wall of the channel when the phase angle ϕ increases, as presented in Figure 2(d).

4.2. Pressure rise and pressure gradient

The pumping characteristics against the dimensionless flow rate for changing the values of Hartmann number M, Darcy number Da, Jeffrey fluid parameter λ_1, and Frude number Fr are presented in Figure 3(a)–(d). Pressure rise is enhanced in the retrograde region ($\Theta < 0, \Delta p_\lambda > 0$) and decreases in co-pumping region ($\Theta > 0, \Delta p_\lambda < 0$) for increasing of Hartmann number and λ_1. But in the peristaltic pumping region ($\Theta > 0, \Delta p_\lambda > 0$), pressure rise increased up to $\Theta \in [0, 0.1]$ and diminished for $\Theta > 0.1$, but opposite behavior is observed for large values of Da (Darcy number). Pressure rise decreases throughout the region (Retrograde region, pumping region, and co-pumping region) when the values of Frude number Fr are enhanced. Pressure gradient for different values of M, Jeffrey fluid parameter λ_1, and Frude number Fr are illustrated in Figure 4(a)–(c). Pressure gradient $\frac{dp}{dx}$ rises throughout the channel for large values of M and Frude number (see Figure 4(a) and (c)). The pressure gradient against the Jeffrey fluid parameter λ_1 is represented in Figure 4(b). From this figure, we observe that the pressure rise diminishes when $x \in [0.6, 0.8]$ and enhances rest of the region.

4.3. Heat and mass transfer

Variations of temperature distribution for Hartmann number M, Darcy number Da Jeffrey fluid parameter λ_1, slip parameter β, and Brinkmann number Br are illustrated in Figure 5(a)–(e). For greater values of M (Hartmann number), the temperature of the fluid increases (see Figure 5(a)). This figure shows that

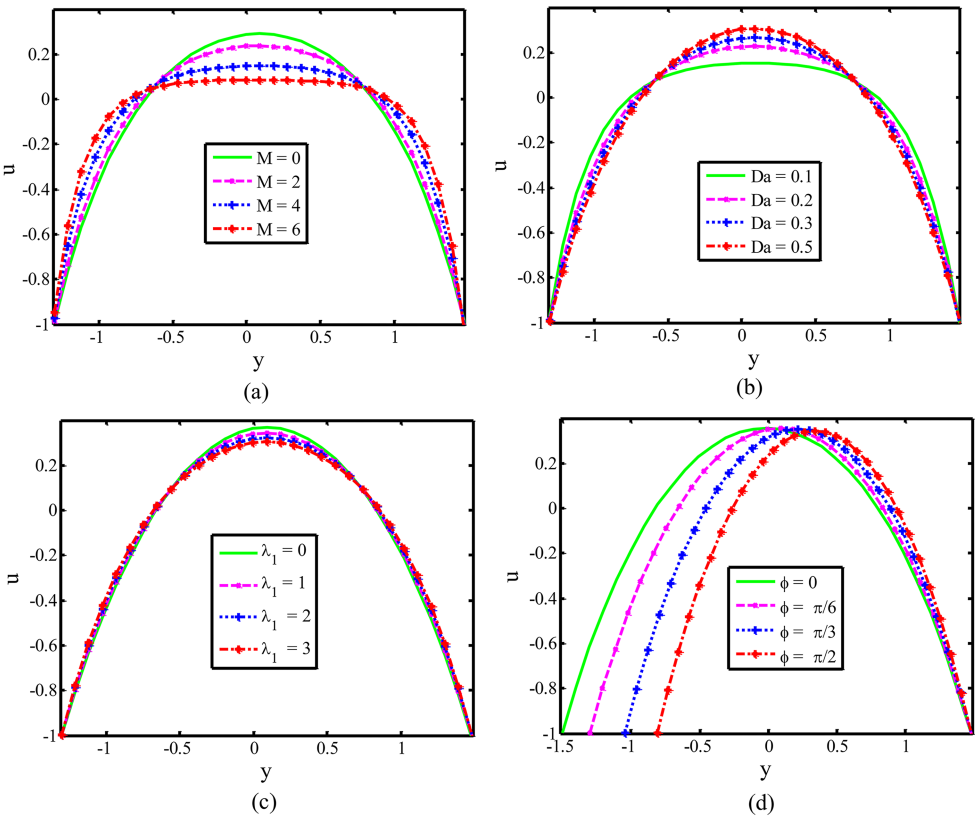

Figure 2. Velocity distribution for (a) $\phi = \frac{\pi}{6}$, $\lambda_1 = 0.2$, $Da = 0.4$, (b) $\phi = \frac{\pi}{6}$, $\lambda_1 = 0.2$, $M = 0.2$, (c) $\phi = \frac{\pi}{6}$, $Da = 2$, $M = 0.5$, (d) $Da = 2$, $\lambda_1 = 0.5$, $M = 0.5$, and other values are $d = 1.1$, $a = 0.6$, $x = 0.1$, $b = 0.5$, $\bar{\eta}_1 = 0.002$, $\bar{\eta}_2 = 0.003$, $\Theta = 1.9$, $l = \frac{\pi}{4}$.

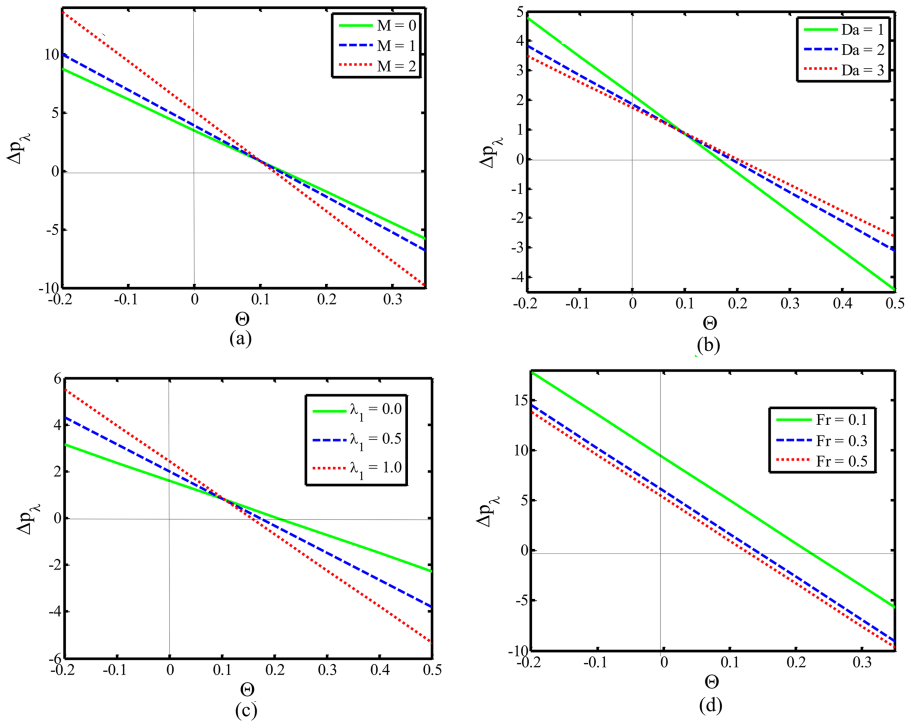

Figure 3. Variation of pressure rise (a) $\lambda_1 = 0.7$, $Da = 0.2$, $Fr = 0.6$, (b) $\lambda_1 = 0.7$, $Fr = 0.6$, $M = 1.5$, (c) $Da = 1$, $Fr = 0.6$, $M = 1.5$, (d) $Da = 0.2$, $\lambda_1 = 0.7$, $M = 2$ and other values are $d = 1.1$, $a = 0.4$, $b = 0.3$, $\phi = \frac{\pi}{6}$, $\bar{\eta}_1 = 0.4$, $\bar{\eta}_2 = 0.5$, $l = \frac{\pi}{6}$, $Re = 0.4$, $\alpha = 0.2$.

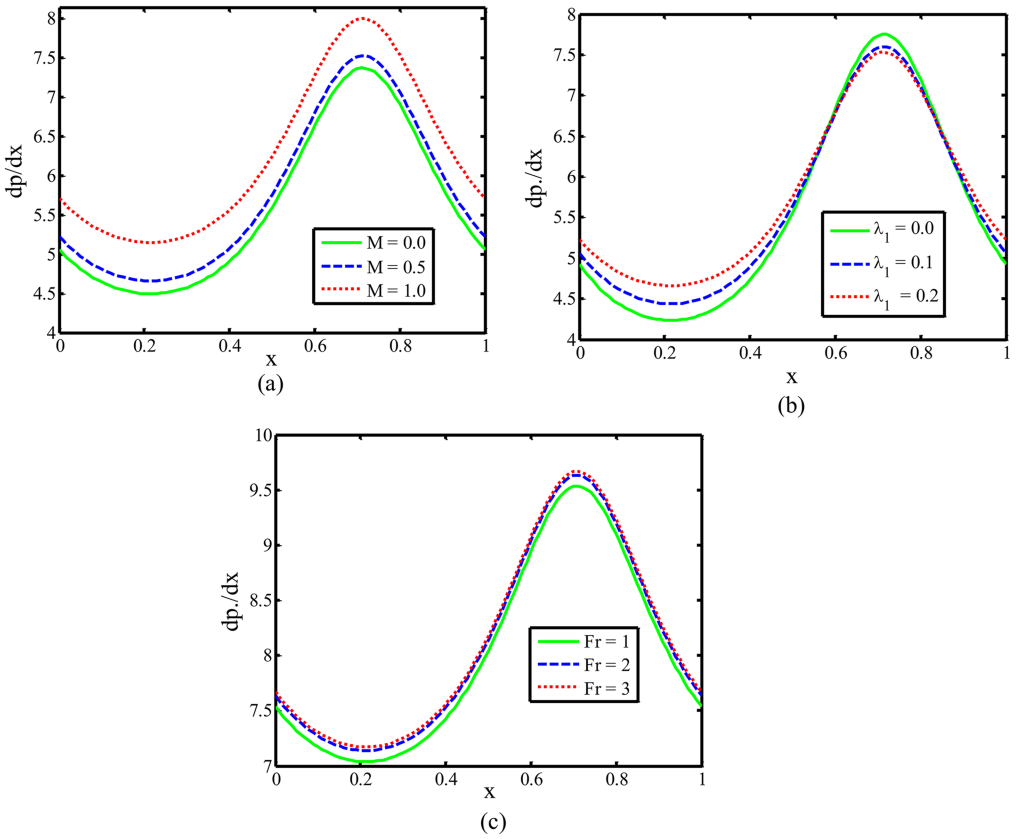

Figure 4. Variation of pressure gradient (a) $Fr = 0.5$, $\lambda_1 = 0.7$, (b) $Fr = 0.6$, $M = 1.5$, (c) $M = 1.5$, $Fr = 0.6$ and other values are $d = 1.1$, $a = 0.4$, $b = 0.3$, $\phi = \frac{\pi}{6}$, $\bar{\eta}_1 = 0.4$, $\bar{\eta}_2 = 0.5$, $\alpha = 0.2$, $l = \frac{\pi}{6}$, $Da = 0.2$, $Re = 0.3$.

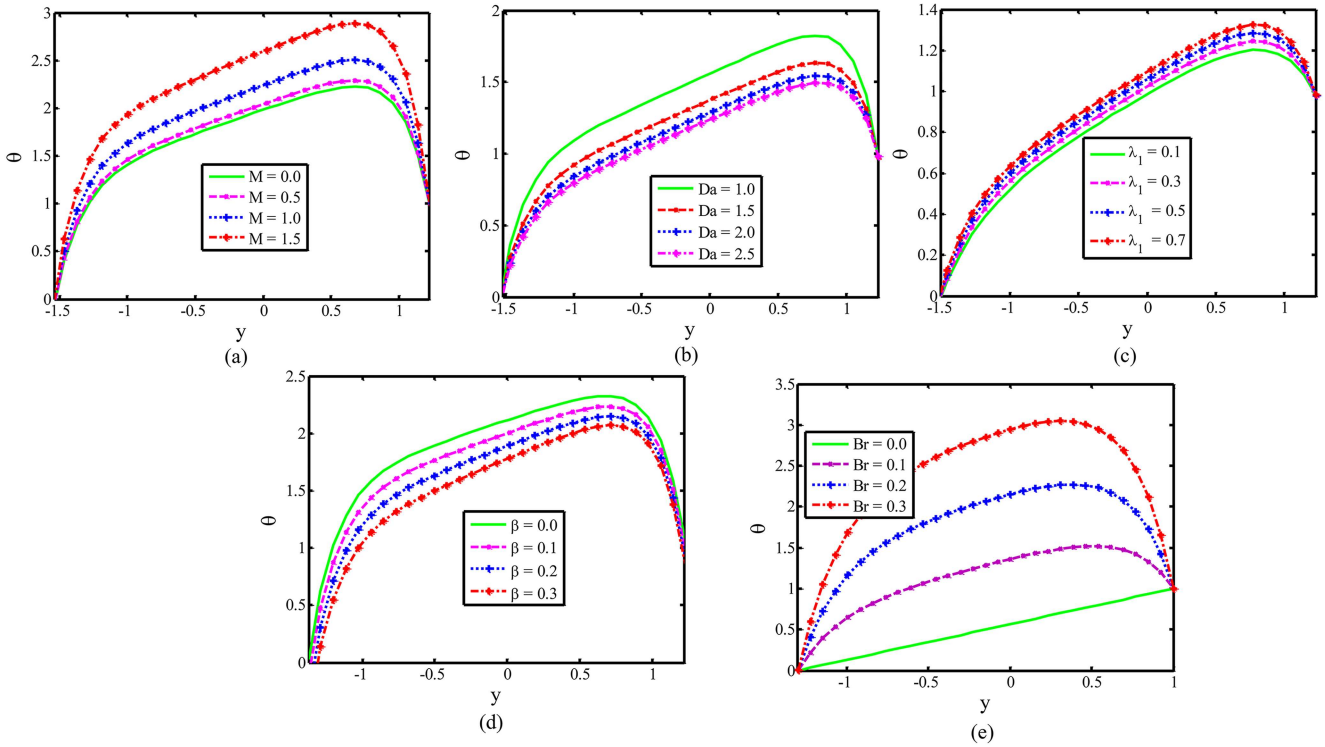

Figure 5. Temperature distribution for (a) $\lambda_1 = 0.3$, $Da = 0.2$, $\beta = Br = 0.1$, (b) $\lambda_1 = 0.3$, $M = 2$, $\beta = Br = 0.1$, (c) $Da = 0.7$, $M = 1.5$, $\beta = Br = 0.1$, (d) $Da = 0.2$, $M = 2$, $\lambda_1 = 0.5$, $Br = 0.1$, (e) $M = 2$, $Da = \lambda_1 = 0.5$, $\beta = 0.01$ and other values are $d = 1.1$, $a = 0.4$, $x = 0.1$, $b = 0.5$, $\phi = \frac{\pi}{6}$, $\bar{\eta}_1 = 0.01$, $\bar{\eta}_2 = 0.02$, $\Theta = 1.9$, $l = \frac{\pi}{4}$.

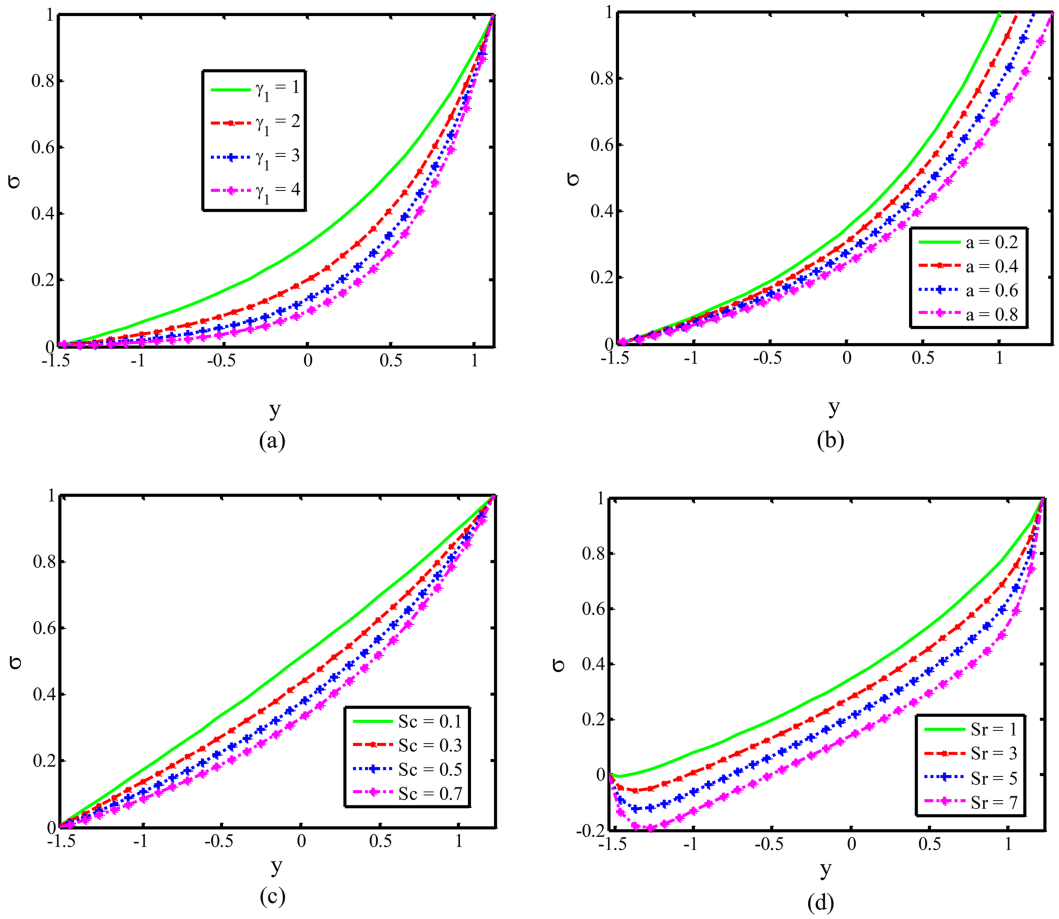

Figure 6. Concentration distribution for (a) $a = 0.4$, $Sr = 0.5$, $Sc = 1$, $\gamma = 0.1$, (b) $Sc = 1$, $Sr = 0.5$, $\gamma = 0.1$, $\gamma_1 = 1$, (c) $a = 0.4$, $Sr = 0.5$, $\gamma = 0.1$, $\gamma_1 = 1$, (d) $a = 0.4$, $Sc = 1$, $\gamma = 0.1$, $\gamma_1 = 1$ and other values are $d = 1.1$, $b = 0.5$, $\phi = \frac{\pi}{6}$, $x = 0.1$, $\bar{\eta}_1 = 0.01$, $\bar{\eta}_2 = 0.02$, $\Theta = 1.9$, $\lambda_1 = 3$, $l = \frac{\pi}{4}$, $M = 2$, $Da = 0.2$, $\beta = 0.01$, $Br = 0.5$.

the temperature of the magnetohydrodynamic fluid is larger when compared to hydrodynamic fluid. The existence of a porous media compensates for the energy dissipation that raises the fluid temperature through internal resistance. Greater values of D_a indicate a decrease in the fluid temperature. The temperature of the fluid increases when λ_1 and Br increase (see Figure 5(c) and (e)). The temperature of the fluid decreases when the value of slip parameter β increases (see Figure 2(d)).

Figure 6(a) and (b) was developed to demonstrate how the amplitude (a) and parameter of a chemical reaction (γ_1) affect the concentration profile. The concentration of the fluid decreases when chemical reaction parameters (γ_1) and amplitude (a) are enhanced. Chemical reaction boosts the rate of mass transfer across interfaces, which reduces concentration. The concentration decreases as the Schmidt number (Sc) increases, as shown in Figure 6(c). Schmidt number is used to characterize fluid flows in which there are simultaneous momentum and mass diffusion convection processes. The density of the fluid particles reduces as the Schmidt number (Sc) rises in value. It helps the particles go away faster, thus reducing concentration. For rising values of the Soret number (Sr), a decrease in concentration is seen (see Figure 6(d)).

4.4. Trapping phenomenon

Trapping is an important mechanism for analyzing the peristaltic fluid flow pattern. Streamlines for different values of M and λ_1 are displayed in Figures 7 and 8. Figure 7 depicts that the size of trapped bolus diminishes in the lower wall for increasing the Hartmann number (M). In both walls of the channel trapped bolus size decreases for large values of λ_1. Finally, the trapped bolus disappears in both walls for increasing the values of Jeffrey fluid parameter λ_1 see Figure 8. Different waveforms of the streamlines, such as sawtooth wave, square wave, trapezoidal wave, and triangular wave, are presented in Figure 9. Present study is validated with the previous study conducted by Misra and Rao [31] with ($M = 0, Da \to \infty, \alpha = 0$). From this figure, we conclude that the present study is in accordance with the existing literature (see Figure 10).

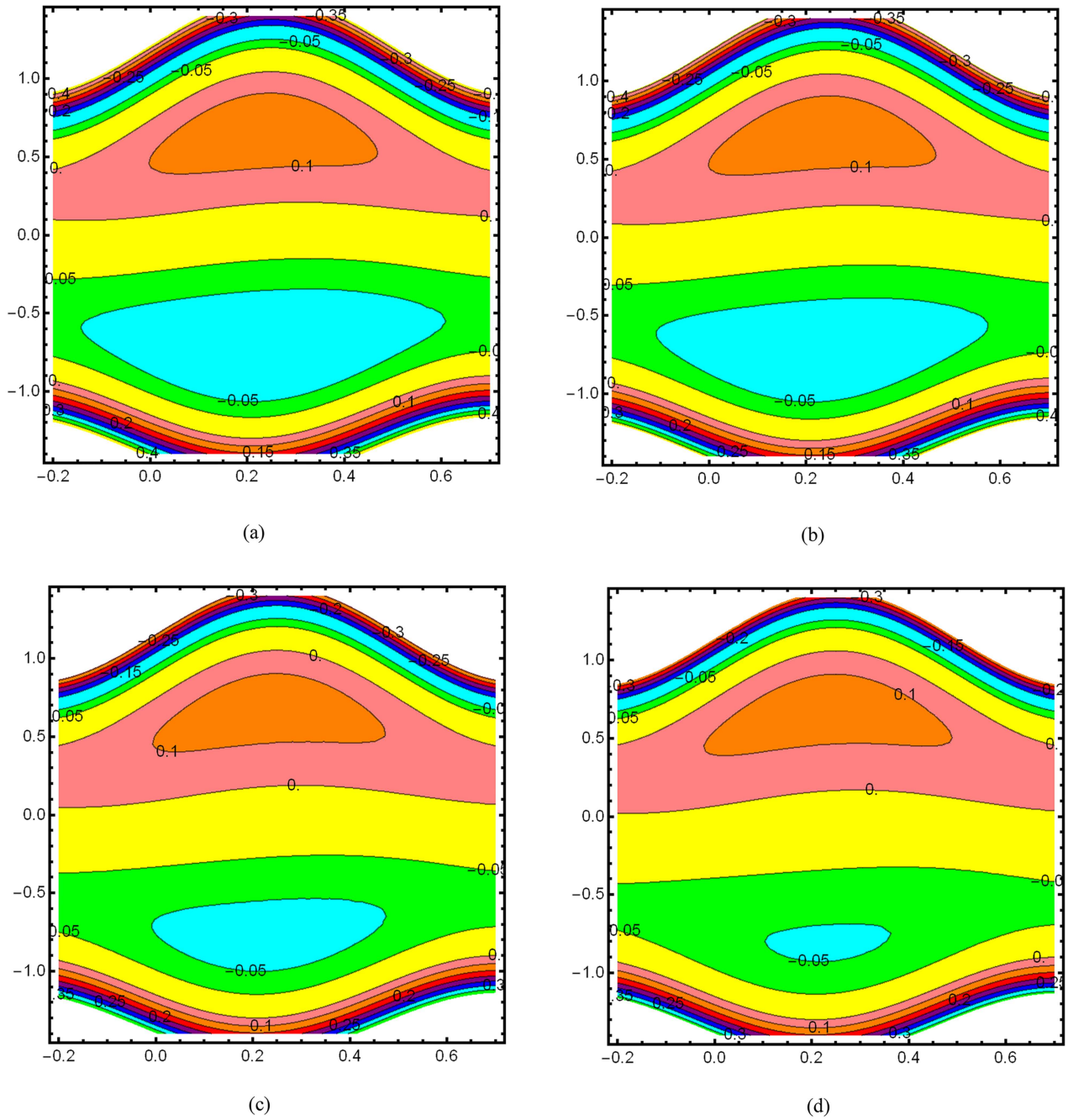

Figure 7. Streamlines for $(a)M = 0$, $(b)M = 1$, $(c)M = 2$, $(d)M = 3$ and other values are $d = 1.1$, $a = 0.4$, $b = 0.5$, $\phi = \frac{\pi}{12}$, $x = 0.1$, $\bar{\eta}_1 = 0.01$, $\bar{\eta}_2 = 0.02$, $\Theta = 1.9$, $\lambda_1 = 0.2$, $l = \frac{\pi}{4}$, $Da = 0.3$.

5. Conclusion

In this study, we investigated the influence of velocity slip conditions on the peristaltic motion of the Jeffrey fluid in the asymmetric channel with porous medium, magnetic field, and chemical reactions. The governing equations are reduced long wavelength and the small Reynolds number approximations. The resulting governing equations are solved by the exact solution. The key findings are as follows:

1. The axial velocity decreases for increasing M, λ_1, and ϕ, but the opposite trend is observed for increasing Da;
2. The pressure rise rises in the pumping region for greater values of M, λ_1, and decreases for Da;
3. Pressure rise decreases throughout the region for increasing Fr;
4. The temperature rises when increasing M, λ_1,

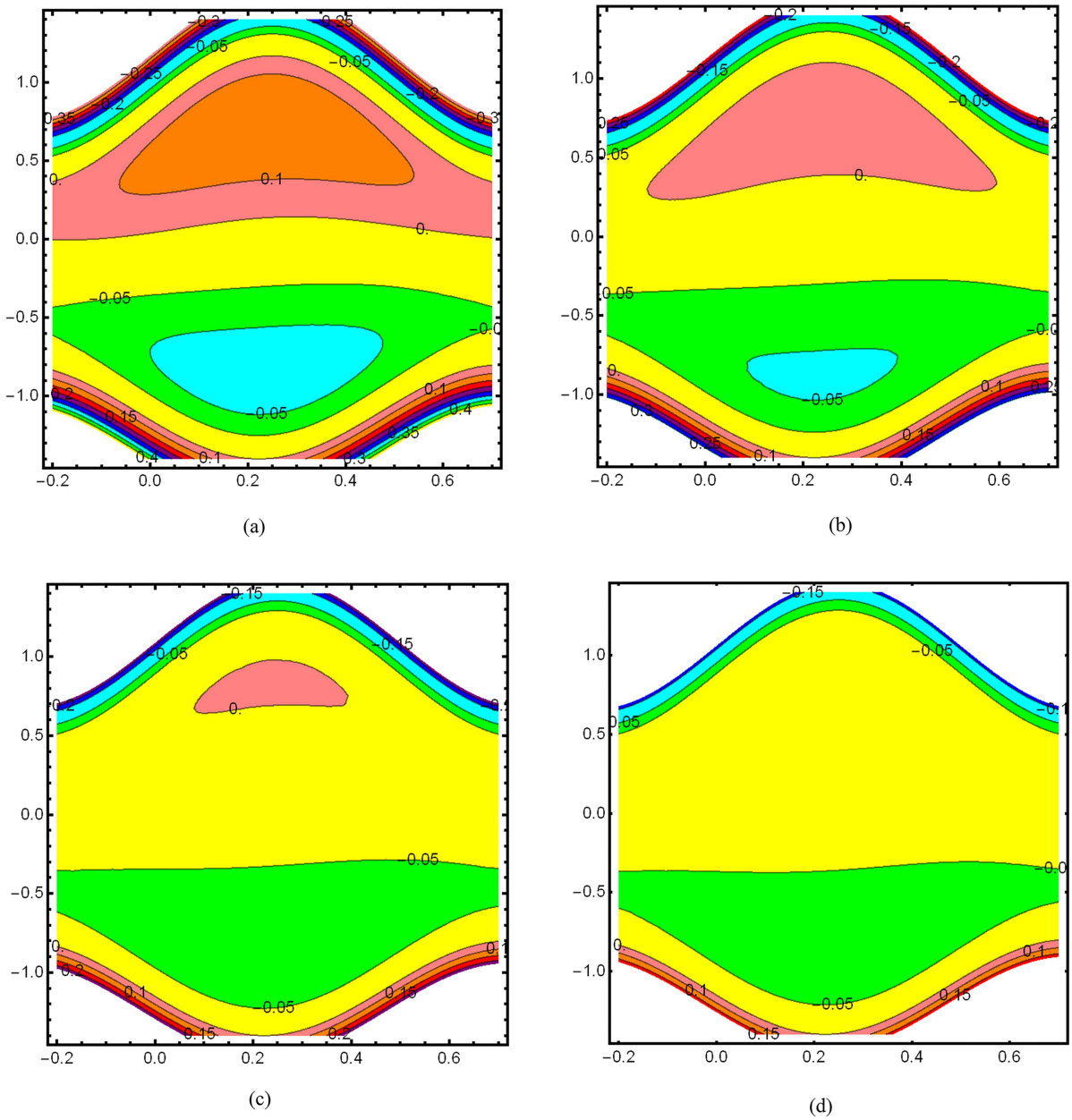

Figure 8. Streamlines for (a) $\lambda_1 = 0$, (b) $\lambda_1 = 1$, (c) $\lambda_1 = 2$, and (d) $\lambda_1 = 3$ other values are $d = 1.1$, $a = 0.4$, $b = 0.3$, $\phi = \frac{\pi}{18}$, $x = 0.1$, $\bar{\eta}_1 = 0.01$, $\bar{\eta}_2 = 0.02$, $\Theta = 1.9$, $M = 1.5$, $l = \frac{\pi}{6}$, $Da = 0.2$.

and Br, but the opposite trend is observed for increasing Da and β;

5. The concentration of the fluid diminished for increasing γ_1, a, Sc, and Sr;
6. The size of the trapped bolus diminishes for larger values of M and λ_1.

Nomenclature

Symbols

$\bar{h}_1, \bar{h}_2$	Upper and lower walls [L]
$u = (\widehat{U}', \widehat{V}')$	Velocity vector on $(\widehat{X}', \widehat{Y}')$ direction
I	Identity tensor
B_0	Magnetic field vector
T	Temperature of fluid
S	Cauchy stress tensor
d_1, d_2	Channel wall's constant height [L]
a_1, b_1	Wave amplitudes [L]
c	Wave speed [L/T]
$\widehat{t}'$	Time [T]

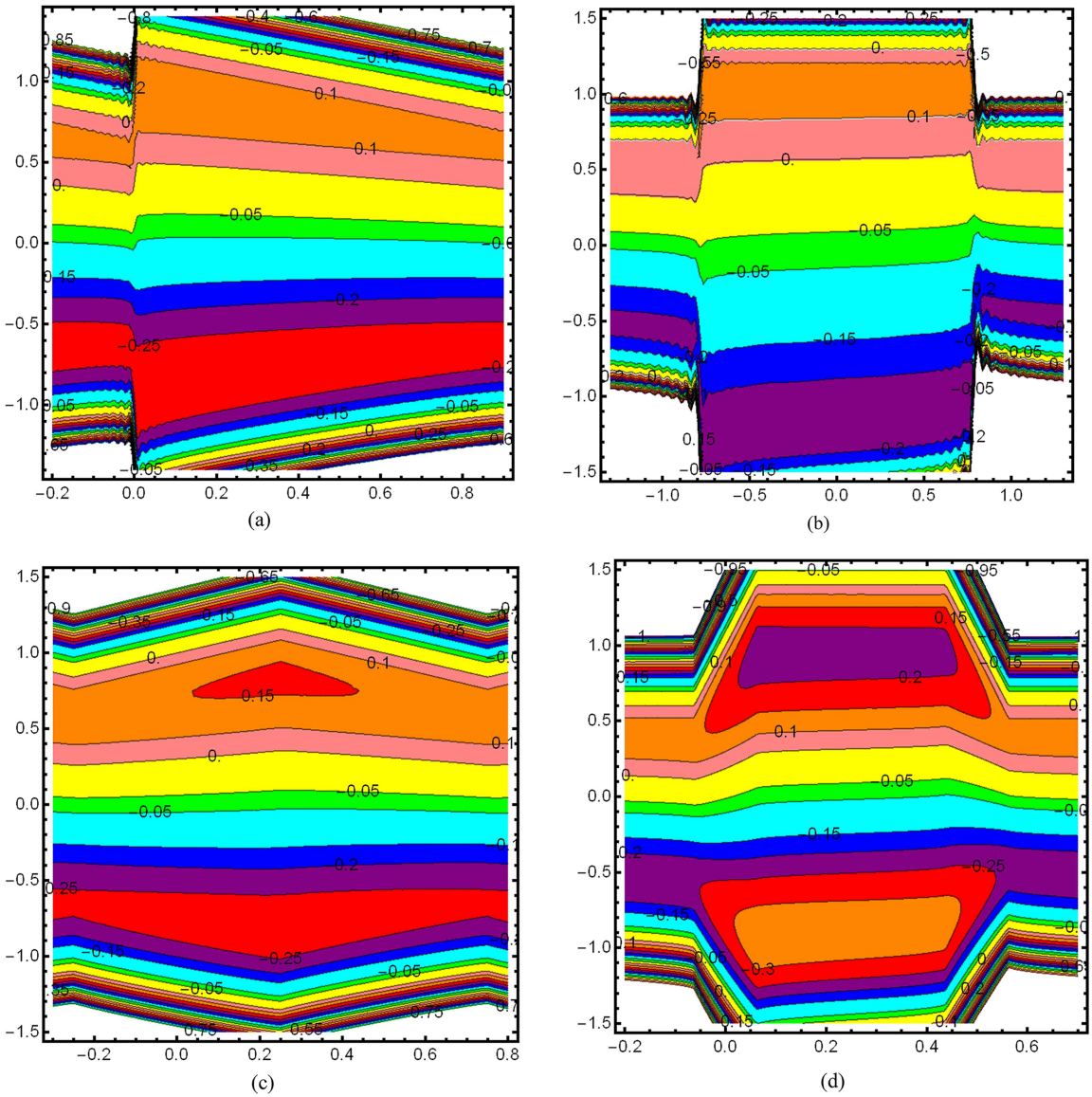

Figure 9. Streamlines for (a) Sawtooth waveform, (b) Square waveform, (c) Triangular waveform, and (d) Trapezoidal waveform.

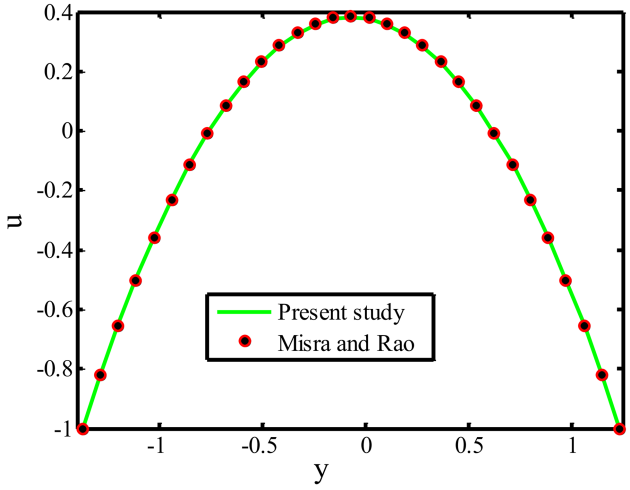

Figure 10. Validation with Misra and Rao [31].

P	Pressure [ML/T^2]
c_p	Specific heat [ML^2/T^{2}K]
k_1	Permeability parameter
T_0, T_1	Temperature at lower and upper wall [K]
Re	Reynolds number
Da	Darcy number
Fr	Frude number
Pr	Prandtl number
M	Hartmann number
E	Eckert number
Br	Brinkmann number
F	Flow rate [M/L^3]

Greek symbols

λ_1, λ_2	Constants of Jeffrey fluid
$\dot{\gamma}, \ddot{\gamma}$	Shear stress
λ	Wavelength [L]
ρ	Density [M/L^3]
μ	Dynamic viscosity
σ	Electrical conductivity
δ	Wave number
ψ	Stream function
κ_t	Thermal conductivity [ML/T^{3}K]
α	Inclination angle
$\bar{\eta}_1, \bar{\eta}_2$	First, second order slip parameters
β^*	Thermal slip parameter
γ_1	Chemical reaction parameter

References

1. Latham, T.W. "Fluid motion in a peristaltic pump", MS Thesis. Cambridge M.A: MIT (1966).
2. Brown,T.D. and Hung, T.K. "Computational and experimental investigation of two-dimensional nonlinear peristaltic flow", *J. Fluid Mech.*, **83**, pp. 249–273 (1977). DOI: 10.1017/S0022112077001189
3. Vajravelu, K., Sreenadh, S., and Babu, V.R. "Peristaltic transport of Herschel-Bulkley fluid in an inclined tube", *J. Nonlinear Mech.*, **40**, pp. 83–90 (2005). DOI: 10.1016/j.ijnonlinmec.2004.07.001
4. Wang, Y., Hayat, T., and Hutter, K. "Peristaltic flow of a Johnson Segalman fluid through a deformable tube", *Theor Comput Fluid Dyn.*, **21**, pp. 369–380 (2007). DOI 10.1007/s00162-007-0054-1
5. Bhatti, M.M. and Abdelsalam, S.I. "Bio-inspired peristaltic propulsion of hybrid nanofluid flow with Tantalum (Ta) and Gold (Au) nanoparticles under magnetic effects", *Waves in Random and Complex Media* (2021). DOI: 10.1080/17455030.2021.1998728
6. Magesh, A., Kothandapani, M., and Pushparaj, V. "Electro-osmotic flow of Jeffry fluid in an asymmetric micro channel under the effect of magnetic field", *J Phys: Conf Ser.*, **1850**, 012102 (2021). DOI: 10.1088/1742-6596/1850/1/012102
7. Magesh, A., Tamizharasi, P., and Vijayaragavan, R. "MHD flow of (Al_2O_3/H_2O) nanofluid under the peristaltic mechanism in an asymmetric channel", *Heat Transf.*, **51**(7), pp. 6563–6577 (2022). DOI: 10.1002/htj.22613
8. Magesh, A., Tamizharasi, P., and Kamalakkannan, J. "Analysis of Bejan number and Entropy generation of Non-Newtonian nanofluid through an asymmetric microchannel", *Numer Heat Transf part A: Appl.* (2023). DOI: 10.1080/10407782.2023.2240507
9. Muthuraj, R., Nirmala, K., and Srinivas, S. "Influences of chemical reaction and wall properties on MHD Peristaltic transport of a Dusty fluid with Heat and Mass transfer", *Alexandr Eng J.*, **55**, pp. 597–611 (2016). DOI: 10.1016/j.aej.2016.01.013
10. Magesh, A., Praveen Kumar, P., Tamizharasi, P., et al. "Effect of magnetic field on the peristaltic transport of Oldroyd-B fluid in an asymmetric inclined channel", *J Phys: Conf Ser.*, **1850**, 012111 (2021). DOI: 10.1088/1742-6596/1850/1/012111
11. Tamizharasi, P., Vijayaragavan, R., and Magesh, A. "Electro-osmotic driven flow of Eyring Powell nanofluid in an asymmetric channel", *Math Methods Appl Sci.*, pp. 1–18 (2023). DOI 10.1002/mma.9270
12. Tamizharasi, P., Vijayaragavan, R., and Magesh, A. "Heat and Mass transfer analysis of the peristaltic driven flow of nanofluid in an asymmetric channel", *Partial Diff Equ Appl Math.*, **4**, 100087 (2021). DOI: 10.1016/j.padiff.2021.100087
13. Magesh, A. and Kothandapani, M. "Analysis of heat and mass transfer on the peristaltic movement of Carreau nanofluids", *J Mech Med Biol.*, **21**(9), 2150068 (2021). DOI: 10.1142/S0219519421500688
14. Rabeeah, R., Rahila, N., and Sara I. Abdelsalam. "Microorganisms swimming through radiative Sutterby nanofluid over stretchable cylinder: Hydrodynamic effect", *Numer. Methods Partial Differential Equations.*, **39**(2), pp. 975–994 (2023). DOI: 10.1002/num.22913
15. Darcy, H., *Les Fontaines Publiques De La Ville De Dijon*, Paris: Dalmont (1856).
16. Mekheimer, Kh.S. "Non-linear peristaltic transport through a porous medium in an inclined planner channel", *J Por Media*, **6**, pp. 189–201 (2003). DOI: 10.1615/JPorMedia.v6.i3.40
17. Sheikholeslami, M., Hatami, M., and Ganji, D.D. "Analytical investigation of MHD nanofluid flow in a semi-porous channel", *Powder Technol*, **246**, pp. 327–336 (2013). DOI: 10.1016/j.powtec.2013.05.030
18. Patil, P.M. and Chamkha, A. "Heat and mass transfer from mixed convection flow of polar fluid along a plate in porous media with chemical reaction", *Int. J. Numer Methods Heat Fluid Flow*, **23**, pp. 899–926 (2013). DOI: 10.1108/HFF-03-2011-0060

19. Gnaneswara Reddy, M. and Venugopal Reddy, K. "Impact of velocity slip and joule heating on MHD peristaltic flow through a porous medium with chemical reaction", *J. Niger Mathematical Society*, **35**, pp. 227–244 (2016). DOI: 10.1016/j.jnnms.2016.02.005

20. Eldesoky, I.M., Abdelsalam, S.I., Wageeh A. El-Askary., et al. "The integrated thermal effect in conjunction with slip conditions on peristaltically induced particle-fluid transport in a catheterized pipe", *J. Por. Media*, pp. 695–713 (2020). DOI: 10.1615/JPorMedia.2020025581

21. Khan, Z.H., Makinde, O.D., Hamid, M., et al. "Hydromagnetic flow of ferrofluid in an enclosed partially heated trapezoidal cavity filled with a porous medium", *J. Magn.Magn. Mater.*, **499**, p. 166241 (2020). DOI: 10.1016/j.jmmm.2019.166241

22. Kamalakkannan, J., Dhanapal, C., Kothandapani, M., et al. "Peristaltic transport of non-Newtonian nanofluid through an asymmetric microchannel with electroosmosis and thermal radiation effects", *Indian J Phys.*, **97**, pp. 2735–2744 (2023). DOI: 10.1007/s12648-023-02636-9

23. Abdelsalam, S.I., Magesh, A., Tamizharasi, P., et al. "Versatile response of a Sutterby nanofluid under activation energy through an asymmetric conduit: Hyperthermia therapy", *Int. J. Numer. Methods Heat Fluid Flow*, **34**(2), pp. 408–428 (2023). DOI: 10.1108/HFF-04-2023-0173

24. Vijayaragavan, R., Tamizharasi, P., and Magesh, A. "Brownian motion and thermoporesis effects of nanofluid flow through the peristaltic mechanism in a vertical channel", *J Por Media.*, **25**(6), pp. 65–81 (2022). DOI: 10.1615/JPorMedia.2022041521

25. Bhatti, M.M., Arain, M.B., Zeeshan, A., et al. "Swimming of Gyrotactic Microorganism in MHD Williamson nanofluid flow between rotating circular plates embedded in porous medium: Application of thermal energy storage", *J. Energy Storage*, **45**, p. 103511 (2022). DOI: 10.1016/j.est.2021.103511

26. Nadeem, S., Riaz, A., Ellahi, R., et al. "Mathematical model for the peristaltic flow of Jeffrey fluid with nanoparticles phenomenon through a rectangular duct", *Appl. Nanosci.*, **4**(5), pp. 613–624 (2014). DOI: 10.1007/s13204-013-0238-5.

27. Bhatti, M.M., Zeeshan, A., and Ellahi, R. "Simultaneous effects of coagulation and variable magnetic field on peristaltically induced motion of Jeffrey nanofluid containing gyrotactic microorganism", *Microvasc Research*, **110**, pp. 32–42 (2017). DOI: 10.1016/j.mvr.2016.11.007

28. Bhatti, M.M., Alamri, S.Z., Ellahi, R., et al. "Intrauterine particle-fluid motion through a compliant asymmetric tapered channel with heat transfer", *J. Therm. Anal. Calorim.*, **144**, pp. 2259–2267 (2021). DOI: 10.1007/s10973-020-10233-9

29. Magesh, A. and Kothandapani, M. "Heat and mass transfer analysis on non-Newtonian fluid motion driven by peristaltic pumping in an asymmetric curved channel", *Eur. Phys. J. Spec. Top.*, **230**, pp. 1447–1464 (2021). DOI: 10.1140/epjs/s11734-021-00035-x

30. Saleem, N., Akram, S., Afzal, F., et al. "Impact of velocity second slip and inclined magnetic field on peristaltic flow coating with Jeffrey fluid in tapered channel", *Coatings*, **10**, p. 30 (2020). DOI: 10.3390/coatings10010030

31. Mishra, M. and Rao, A.R. "Peristaltic transport of a Newtonian fluid in an asymmetric channel", *Z. Angew Math Phys.*, **54**, pp. 532–550 (2003). DOI: 10.1007/s00033-003-1070-7

32. Abd Elmaboud, Y. and Abdelsalam, S.I. "DC/AC magnetohydrodynamic-micropump of a generalized Burger's fluid in an annulus", *Phys Scr.*, **94**, p. 115209 (2019). DOI: 10.1088/1402-4896/ab206d

33. Bhatti, M.M. and Abdelsalam, S.I. "Thermodynamic entropy of a magnetized Ree-Eyring particle-fluid motion with irreversibility process: A mathematical paradigm", *J Appl Math Mech.*, **101**(6), pp. 1–17 (2021). DOI: 10.1002/zamm.202000186

Appendix

$$A_1^2 = (1+\lambda_1)\left[M^2\cos^2\theta + \frac{1}{Da}\right],$$

$$A_2 = A_1 \sinh A_1 h_1 + \frac{\eta_1}{(1+\lambda_1)} A_1^2 \cosh A_1 h_1 + \frac{\eta_2}{(1+\lambda_1)} A_1^3 \sinh A_1 h_1,$$

$$A_3 = A_1 \cosh A_1 h_1 + \frac{1}{(1+\lambda_1)}\left[\eta_1 A_1^2 \sinh A_1 h_1 + \eta_2 A_1^3 \cosh A_1 h_1\right],$$

$$A_4 = A_1 \sinh A_1 h_2 - \frac{1}{(1+\lambda_1)}\left[\eta_1 A_1^2 \cosh A_1 h_2 + \eta_2 A_1^3 \sinh A_1 h_2\right],$$

$$A_5 = A_1 \cosh A_1 h_2 - \frac{1}{(1+\lambda_1)}\left[\eta_1 A_1^2 \sinh A_1 h_2 + \eta_2 A_1^3 \cosh A_1 h_2\right],$$

$$A_6 = h_2 - h_1, \qquad A_7 = \cosh A_1 h_2 - \cosh A_1 h_1,$$

$$A_8 = \sinh A_1 h_2 - \sinh A_1 h_1, \qquad A_9 = A_4 - A_2,$$

$$A_{10} = A_5 - A_3, \qquad A_{11} = A_7 - A_4 A_6,$$

$$A_{12} = A_8 - A_5 A_6, \qquad c_4 = \frac{(F + A_6)\, A_9}{A_{12} A_9 - A_{10} A_{11}},$$

$$c_3 = -c_4 \frac{A_{10}}{A_9},$$

$$c_2 = -1 - c_3 A_4 - c_4 A_5,$$

$$c_1 = \frac{F}{2} - c_2 h_2 - c_3 \cosh A_1 h_2 - c_3 \sinh A_1 h_2,$$

$$A_{14} = -A_{13} \left(\frac{c_3^2}{4} + \frac{c_4^2}{4} + \frac{c_3 c_4}{2} \right),$$

$$A_{15} = -A_{13} \left(\frac{c_3^2}{4} + \frac{c_4^2}{4} - \frac{c_3 c_4}{2} \right),$$

$$A_{16} = -2A_{13} \left(\frac{c_3^2}{4} - \frac{c_4^2}{4} \right),$$

$$A_{17} = \frac{A_{14} e^{2A_1 h_1}}{4A_1^2} + \frac{A_{15} e^{-2A_1 h_1}}{4A_1^2} + \frac{A_{16} h_1^2}{2} + \beta \left[\frac{A_{14} e^{2A_1 h_1}}{2A_1} - \frac{A_{15} e^{-2A_1 h_1}}{2A_1} + A_{16} h_1 \right],$$

$$A_{18} = \frac{A_{14} e^{2A_1 h_2}}{4A_1^2} + \frac{A_{15} e^{-2A_1 h_2}}{4A_1^2} + \frac{A_{16} h_2^2}{2} - \beta \left[\frac{A_{14} e^{2A_1 h_2}}{2A_1} - \frac{A_{15} e^{-2A_1 h_2}}{2A_1} + A_{16} h_2 \right],$$

$$c_6 = \frac{1 + A_{17} - A_{18}}{A_6 - 2\beta}, \quad c_5 = -\left(A_{17} + c_6 \left(h_1 + \beta \right) \right),$$

$$l_1 = \cosh \left(\sqrt{Sc\gamma_1} h_1 \right) + \gamma \sqrt{Sc\gamma_1} \sinh \left(\sqrt{Sc\gamma_1} h_1 \right),$$

$$l_2 = \sinh \left(\sqrt{Sc\gamma_1} h_1 \right) + \gamma \sqrt{Sc\gamma_1} \cosh \left(\sqrt{Sc\gamma_1} h_1 \right),$$

$$l_3 = -ScSr \left(\frac{A_{14} e^{2A_1 h_1} (1 + 2A_1 \gamma) + A_{15} e^{-2A_1 h_1} (1 - 2A_1 \gamma)}{4A_1^2 - Sc\gamma_1} - \frac{A_{16}}{Sc\gamma_1} \right),$$

$$l_4 = \cosh \left(\sqrt{Sc\gamma_1} h_2 \right) + \gamma \sqrt{Sc\gamma_1} \sinh \left(\sqrt{Sc\gamma_1} h_2 \right),$$

$$l_5 = \sinh \left(\sqrt{Sc\gamma_1} h_2 \right) + \gamma \sqrt{Sc\gamma_1} \cosh \left(\sqrt{Sc\gamma_1} h_2 \right),$$

$$l_6 = -ScSr \left(\frac{A_{14} e^{2A_1 h_2} (1 + 2A_1 \gamma) + A_{15} e^{-2A_1 h_2} (1 - 2A_1 \gamma)}{4A_1^2 - Sc\gamma_1} - \frac{A_{16}}{Sc\gamma_1} \right),$$

$$c_7 = -(l_2 c_8 + l_3)/l_1,$$

$$c_8 = \frac{l_3 l_4 + l_1 - l_1 l_6}{l_1 l_5 - l_2 l_4}.$$

Biographies

Rajaram Vijayaragavan is working as a Professor of Mathematics at Thirvalluvar University, Vellore, Tamilandu, India. He obtained his MSc, MPhil, and PhD degrees from the University of Madras. He published many papers in the reputed international journals. His area of interest is computational fluid dynamics.

Perumal Tamizharasi is working as an Assistant Professor of Mathematics at Easwari Engineering College, Ramapuram, Chennai. She obtained her MSc, MPhil and PhD at Thiruvalluvar University, Vellore, India. Her research interest area is Fluid dynamics, especially peristaltic transport, Heat and mass transfer, and nanofluid. She has published more than 10 papers in reputed international journals.

Arjunan Magesh is working as an Assistant Professor in the Department of Mathematics at Sri Sai Ram Engineering College, West Tambaram, Chennai, Tamilnadu, India. He obtained his MSc and MPhil from Thiruvalluvar University and PhD from Anna University, Chennai, India. His area of interest is computational fluid dynamics, particularly curved channels, heat and mass transfer, electroosmosis, porous media, etc. He published more than 15 papers in the reputed international journals. He is the reviewer of some reputed international journals.